ACS NANO

www.acsnano.org

ARTICLE

Self-Organized Freestanding One-Dimensional Au Nanoparticle Arrays

Myungkoo Kang,*[,†,⊥] Yu Yuwen,[†,⊥] Wenchong Hu,[†] Seokho Yun,[†] Krishnamurthy Mahalingam,[‡] Bin Jiang,[§] Kurt Eyink,[‡] Ekaterina Poutrina,[‡] Kathleen Richardson,[∥] and Theresa S. Mayer*[,†]

[†]Department of Electrical Engineering, Pennsylvania State University, University Park, Pennsylvania 16802, United States

[‡]Air Force Research Laboratory, Materials and Manufacturing Directorate (AFRL/RXAN), Wright-Patterson AFB, Dayton, Ohio 45433-7707, United States

[§]FEI Company, Hillsboro, Oregon 97124, United States

[∥]CREOL, College of Optics and Photonics, University of Central Florida, Orlando, Florida 32816, United States

Supporting Information

ABSTRACT: One-dimensional Au nanoparticle arrays encapsulated within freestanding SiO_2 nanowires are fabricated by thermal oxidation of Au-coated Si nanowires with controlled diameter and surface modulation. The nanoparticle diameter is determined by the Si nanowire diameter and Au film thickness, while the interparticle spacing is independently controlled by the Si nanowire modulation. The optical absorption of randomly oriented Au nanoparticle arrays exhibits a strong plasmonic response at 550 nm. Scanning transmission electron microscopy (STEM)−electron energy loss spectrum (EELS) of nanoparticle arrays confirmed the same plasmonic response and demonstrated uniform optical properties of the Au nanoparticles. The plasmonic response in the STEM-EELS maps is primarily confined around the vicinity of the nanoparticles. On the other hand, examination of the same nanowires by energy-filtered transmission electron microscopy also revealed significant enhancement in the plasmonic excitation in the regions in between the nanoparticles. This versatile route to synthesize one-dimensional Au nanoparticle arrays with independently tailorable nanoparticle diameter and interparticle spacing opens up opportunities to exploit enhanced design flexibility and cost-effectiveness for future plasmonic devices.

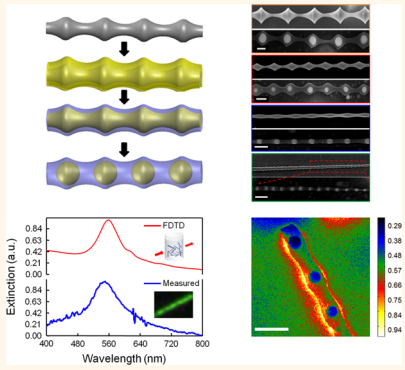

KEYWORDS: *Au nanoparticle arrays, SiO_2 nanowires, thermal oxidation, surface modulation, plasmon*

Plasmonic nanoparticle arrays are promising for a broad range of applications, including biosensors,[1] surface-enhanced Raman spectroscopy,[2] waveguides,[3] nano-antennas,[4] and negative index materials.[5] The array properties are based on electromagnetic field enhancement at the metal−nanoparticle surface, which is controlled by the nanoparticle array material and geometry, the dielectric constant of the surrounding media, and the wave polarization and direction.[3,6] For example, one-dimensional plasmonic nanoparticle arrays with a small interparticle spacing in the near-field coupling regime allow the electromagnetic wave to propagate below the diffraction limit and through 90° bends without significant loss,[3] making these structures well-suited for waveguides. In contrast, particle arrays with a large interparticle spacing can have sharp plasmonic peaks through far-field interparticle coupling,[6] offering high sensitivity for sensors.

A variety of nanofabrication processes have been demonstrated to produce planar and freestanding plasmonic nanoparticle arrays with tailored geometries.[6−26] The most commonly used method for fabricating nanoparticle arrays on planar substrates uses electron-beam lithography, metal evaporation, and lift-off.[6] A range of array geometries is enabled through the patterning and deposition process, while the process is often not scalable nor cost-effective. Alternative methods that create nanoparticles by annealing planar[7] or patterned[8] Au thin films coated on Si substrates reduce cost, but they produce arrays with limited control over nanoparticle diameter and interparticle spacing. Several maskless processes that combine the top-down and bottom-up hybrid approaches were utilized to dewet and transform surface metallic layers into metallic nanostructure arrays, providing a greater flexibility for the array geometry.[9−15] However, these approaches still face barriers toward large-scale device production. Solution-based nanoparticle assembly through linker molecules[16] also greatly reduces the cost and enables large-scale fabrication, but at the expense of full controllability in the interparticle spacing and uniformity of the particles. Laser heating[17] and in-fiber

Received: March 2, 2017
Accepted: June 5, 2017
Published: June 5, 2017

DOI: 10.1021/acsnano.7b01479
ACS Nano 2017, 11, 5844−5852

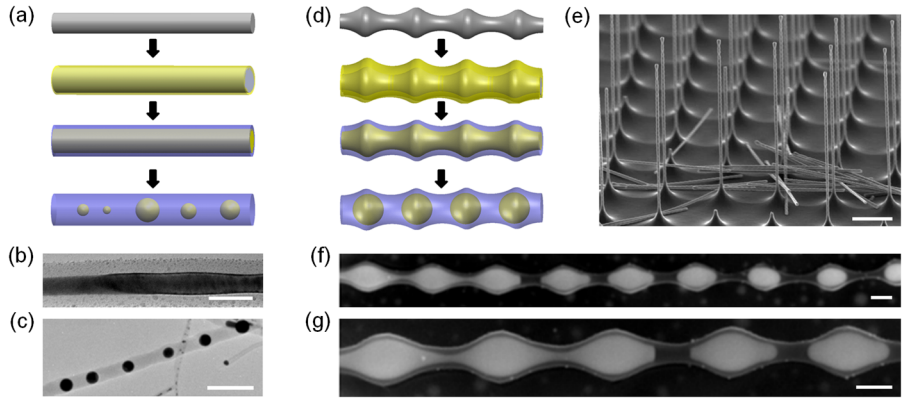

Figure 1. SiO_2-encapsulated Au nanoparticle arrays fabricated by thermal oxidation of Au-coated Si nanowires with smooth (a–c) and modulated (d–g) surfaces. (a) Schematic process for a one-dimensional Au nanoparticle array formed using smooth nanowires. (b) TEM image of a Au nanowire within a SiO_2 shell during oxidation of the 20–50 nm diameter Si nanowire with 10 nm thick Au film. Scale bar, 50 nm. (c) TEM image of a Au nanoparticle array formed within the SiO_2 shell after complete oxidation of the nanowire. Scale bar, 50 nm. (d) Schematic process for a one-dimensional Au nanoparticle array formed using Si nanowires with controlled surface modulation. (e) As-etched array of vertically oriented Si nanowires. (f and g) Evolution of Au nanoparticle array formation inside the SiO_2 nanowire. The starting Si nanowire had a maximum diameter of 200 nm (convex region), a minimum diameter of 80 nm (concave region), a modulation wavelength of 630 nm, a length of 5.6 μm, and a Au layer thickness of 20 nm. Scale bar, 200 nm.

fabrication[18] provide a cost-effective and high-throughput method, but the interparticle spacing has been limited to the micrometer scale. The controlled aggregation of nanoparticles has been enabled by either placing drops of nanoparticles in an aqueous solution on prepatterned trenches[19] or encapsulating aggregates of nanoparticles in polymeric shells.[20] Meanwhile, these methods typically require complex multilevel processing. Au nanoparticle arrays observed in thermally oxidized Si nanowires that were grown by the Au-catalyzed vapor–liquid–solid (VLS) method[21−26] provide better engineering strategies in manipulating diameter and interparticle spacing. However, the Rayleigh instability-driven linear dependence of interparticle spacing on nanoparticle diameter or the simple diffusion process limits fully independent control over diameter and interparticle spacing.

This paper reports a versatile method to synthesize self-organized one-dimensional Au nanoparticle arrays encapsulated within freestanding silicon dioxide (SiO_2) nanowires. This process provides independent and precise control of nanoparticle diameter and interparticle spacing along the length of the wire. This is achieved by thermal oxidation of Au-coated Si nanowires with highly tailorable and reproducible diameter and surface modulation created by deep reactive ion etching (DRIE). The nanoparticle diameters are determined by the volume of the deposited Au film on the surface of the wire, and their interparticle spacing is defined by the surface modulation wavelength of the starting Si nanowire. Optical absorption measurements of a suspension of randomly oriented SiO_2-encapsulated Au nanoparticle arrays with 80 nm diameter particles and 230 nm interparticle spacing showed a plasmonic response with an intense peak at 550 nm. Scanning transmission electron microscopy–electron energy loss spectra (STEM-EELS) of individual nanoparticle array wires confirmed the same plasmonic response and high uniformity in the Au nanoparticle properties. Additional energy-filtered transmission electron microscopy (EFTEM) analysis showed optical coupling between adjacent Au nanoparticles in the array. These results demonstrate that this fabrication method provides a cost-effective and scalable approach to create freestanding one-dimensional nanoparticle array building blocks with increased flexibility for future plasmonic devices including biosensors,[1] surface-enhanced Raman spectroscopy,[2] waveguides,[3] nanoantennas,[4] and negative index materials.[5]

RESULTS AND DISCUSSION

Versatile Route to Synthesize One-Dimensional Au Nanoparticle Arrays. As illustrated in Figure 1, SiO_2-encapsulated Au nanoparticle arrays fabricated by thermal oxidation of Au-coated Si nanowires with smooth and modulated surfaces are compared to show the greatly enhanced control and uniformity in particle diameter and interparticle spacing obtained using surface-modulated wires. In this work, Si nanowires with smooth surfaces were grown by the Au-catalyzed VLS method. Our previous work indicates that an intrinsic variation of Au catalyst size induces a batch of starting Si nanowires to have a distribution of diameters in a single growth,[27] and the values range from 20 to 50 nm in this study. This distribution of starting material geometry allowed rapid analysis of Au nanoparticle arrays as a function of starting wire diameter and volume of deposited Au. In the process illustrated in Figure 1a, the Au catalyst particles were selectively removed from the Si nanowire tips[28] prior to coating the top side of the wires with a uniform 10 nm thick Au film. The Au-coated Si nanowires were then thermally treated in a tube furnace at a temperature of 850 °C under pure, dry O_2 flow. It has been shown previously that the Au weakens the covalent bond between Si atoms and increases the extraction and oxidation rate of Si at the Si–Au interface.[29] For these Au-coated Si nanowires, the movement of Au toward the core of the wire is enhanced to reduce the surface and interfacial free energy. As the Au-enhanced oxidation process advances,[29] each Au-coated Si nanowire is transformed into a crystalline Au nanowire encapsulated in a freestanding SiO_2 nanowire, as shown by the transmission electron microscope (TEM) image in Figure 1b. After complete oxidation of the Si wire, the solid Au nanowire then breaks into a nanoparticle array to reduce the interfacial energy between the Au core and SiO_2 shell, as shown by the TEM image in Figure 1c.[27] The nanoparticle diameter and interparticle spacing for the Au nanoparticle array in Figure 1c varied from 10 to 16 nm and 30 to 47 nm, respectively.

DOI: 10.1021/acsnano.7b01479
ACS Nano 2017, 11, 5844–5852

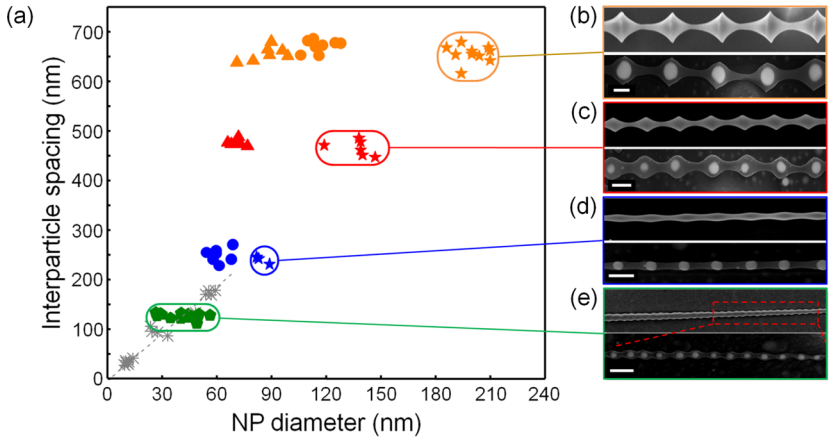

Figure 2. (a) Distribution of Au nanoparticle arrays with controlled interparticle spacing and diameter formed by the same thermal treatment at 850 °C for 2 h. (b–e) Corresponding FESEM images: the top image in each colored box was taken at an accelerating voltage of 5 kV, and the bottom image was taken at an accelerating voltage of 20 kV. All scale bars, 200 nm. Each symbol represents the average of the particle diameter and interparticle spacing within a single wire resulting from the following Au coating thickness/modulation wavelength: (gold star) 20 nm/630 nm; (gold dot) 10 nm/630 nm; (gold triangle) 5 nm/630 nm; (red star) 20 nm/430 nm; (red triangle) 5 nm/430 nm; (blue dot) 10 nm/230 nm; (blue star) 20 nm/230 nm; (green pentagon) tapered nanowires with 10 nm Au coating; (gray asterisk) smooth nanowires with 10 nm Au coating.

The transition of a smooth-surface core metallic nanowire into a one-dimensional nanoparticle array has been reported for several dielectric-encapsulated metallic nanowire systems such as Au/SiO_2, Au/TiO_2, Au/Al_2O_3, Au/Ga_2O_3, and Cu/TiO_2.[30,31] This trend is explained by Rayleigh instability theory which describes the thermodynamic instability of an infinite cylindrical wire due to capillary-induced surface tension.[22] When a modulation wavelength is greater than the circumference of a cylindrical wire, kinetics predicts that the wire is fragmented to a row of particles *via* atomic diffusion to minimize the interfacial energy between the wire and the matrix.[32,33] The atomic diffusion increases with increasing gradient of the curvature of the wire surface. Elevated annealing temperatures typically make the atomic diffusion high enough to overcome the kinetic limitation. The wire ruptures at multiple points along its length and finally becomes fragmented into a row of particles. In the system here, continued thermal treatment following complete oxidation of the Si gives rise to a sinusoidal modulation of the Au nanowire diameter with a wavelength that depends on the starting diameter of the Au wire.[34] The amplitude of the modulation grows with time, ultimately causing the wire to break into an array of spherical Au nanoparticles with an interparticle spacing equal to the modulation wavelength. Rayleigh theory predicts that the modulation wavelength will grow with increasing Au wire diameter. The average particle diameter *versus* interparticle spacing for Au nanoparticle arrays synthesized from smooth Si nanowires with different starting diameter, and consequently Au wire diameter, is shown by the gray symbols in Figure 2a. The dashed gray line in this figure shows that the ratio of the particle diameter to interparticle spacing follows a linear relationship with a slope of 3, which falls within the observed values of 2.3 and 4.5 for the Rayleigh instability.[22,27,35] Therefore, it is not possible to independently tune the nanoparticle diameter and the interparticle spacing on smooth wires because the ratio is fixed, which restricts the use of these wires for plasmonic applications.

The limitation enforced by the Rayleigh instability can be overcome to create one-dimensional arrays with highly tailorable Au nanoparticle diameter and interparticle spacing by introducing controlled modulation in the Au wire diameter during Au-enhanced oxidation. The process demonstrated in this work is illustrated in Figure 1d (see Materials and Methods section and Supporting Information for details). Briefly, nanowire array features were patterned on a thermally oxidized Si substrate using projection lithography and then were transferred vertically into the Si substrate by DRIE, leading to Si nanowires with a uniform diameter and modulated surface. Figure 1e shows an as-etched array of vertically oriented Si nanowires. During DRIE, alternating etching and polymer deposition cycles were optimized to create scalloped profiles (concave- and convex-shaped segment regions) with predefined surface modulation wavelengths along the length of the Si nanowires in the array.[36] Each batch of surface-modulated Si nanowires was then coated with a deposited Au thin film of a specified thickness and thermally treated in a flow of dry O_2. During Au-enhanced oxidation, the Au atoms in the concave region of the Si nanowire migrate to the convex region, which results in a surface-modulated crystalline Au wire, as shown by the field emission scanning electron microscope (FESEM) images in Figure 1f and g. Over a wide range of geometries, the controlled surface modulation introduced by the scalloped Si sidewall overcomes the intrinsic modulation due to the Rayleigh instability. In these cases, the Au wire breaks at the points where its diameter is the narrowest. The initial phase of the fragmentation process is observed in several regions along the wire in Figure 1f and g. Continued thermal treatment of the same batch of wires resulted in well-controlled Au nanoparticle arrays with uniform particle diameters of 200 ± 10 nm and interparticle spacings of 622 ± 17 nm, as shown in the FESEM images of Figure 2b. Our previous work indicates that this trend is consistently observed within an ensemble of nanowires.[37]

Independent and Precise Control of Nanoparticle Diameter and Interparticle Spacing. In this process, the Au nanoparticle diameter and interparticle spacing can be adjusted independently by controlling both the Si nanowire modulation wavelength and the deposited Au layer thickness, as shown by the data plotted in Figure 2. Each symbol in Figure 2 represents the average of the particle diameter and interparticle spacing within a single wire formed by a thermal treatment at 850 °C

DOI: 10.1021/acsnano.7b01479
ACS Nano 2017, 11, 5844–5852

for 2 h. To calculate the diameters and interparticle spacings of the Au nanoparticles in the SiO_2 nanowires, various numbers of nanowires ranging from 4 to 12, which are represented by the number of symbols in each group shown in Figure 2, were taken into account. The gold triangle, circle, and star symbols in Figure 2 compare Au nanoparticle arrays fabricated by fixing the modulation wavelength at 630 nm and varying the deposited Au thickness to 5, 10, and 20 nm. As shown in this plot, the three Au thicknesses produced arrays with tightly controlled interparticle spacings of 637 ± 31 nm and uniform nanoparticle diameters of 88 ± 6, 118 ± 6, and 200 ± 10 nm, respectively. Alternatively, the interparticle spacing can be modified while maintaining the same nanoparticle diameter by tuning the Au thickness and the modulation wavelength. As shown by the gold triangle and blue star symbols, Au nanoparticles with diameters of 85 ± 8 can be fabricated by coating 5 nm of Au on Si nanowires with a modulation wavelength of 630 nm or by coating 20 nm of a Au layer on nanowires with a modulation wavelength of 230 nm.

Finally, nanoparticle arrays with different nanoparticle diameters and interparticle spacings can be made by fixing the Au layer thickness while varying the modulation wavelength, as shown by the FESEM images in Figure 2b–d. For the nanowires with a Au layer thickness of 20 nm and modulation wavelengths of 230, 430, and 630 nm, the nanoparticle diameters are 80 ± 10, 120 ± 19, and 190 ± 10 nm, while the interparticle spacings are 238 ± 21, 435 ± 38, and 622 ± 17 nm, respectively.

This versatile nanofabrication method also allows independent control of the nanoparticle diameter and/or interparticle spacing along the length of the same nanowire. For example, the nanoparticle diameter can be varied while maintaining a fixed interparticle spacing. The top image of Figure 2e shows a tapered Si nanowire with a 130 nm modulation wavelength and a diameter that increases from 65 nm at the top to 125 nm at the bottom of the nanowire. The nanoparticle array formed by Au-enhanced oxidation of the wire after deposition of a 10 nm thick Au layer is shown in the bottom image of Figure 2e. The nanoparticle diameter increases monotonically from 37 nm at the top to 47 nm at the bottom of the nanowire, while the interparticle spacings are maintained at 130 ± 7 nm.

Optical Absorption of Randomly Oriented Nanoparticle Arrays. The plasmonic properties of the one-dimensional Au nanoparticle arrays were characterized by measuring the extinction spectra of a randomly oriented population of 6 μm long nanowire arrays suspended in an isopropyl alcohol (IPA) solution. The spectrum shown in Figure 3a was collected on a batch of wire arrays composed of 80 nm diameter Au nanoparticles with a 230 nm interparticle spacing encapsulated within a 100 nm thick SiO_2 shell. The measurement was conducted using a UV–vis spectrometer (PerkinElmer Lambda 9500) with unpolarized light. The transmitted beam energy was measured and referenced to the incident beam energy to extract the extinction energy. The measured spectrum shows an intense extinction peak at 550 nm. Extinction consists of two distinct processes including scattering and absorption. The ratio of the scattering cross-section to the absorption cross-section is dependent upon the size of metallic nanoparticles and their surrounding medium.[38] To experimentally identify a dominant contribution to the observed optical properties, individual one-dimensional Au nanoparticle arrays were also characterized by dark-field scattering. For this measurement, nanowires were dropped

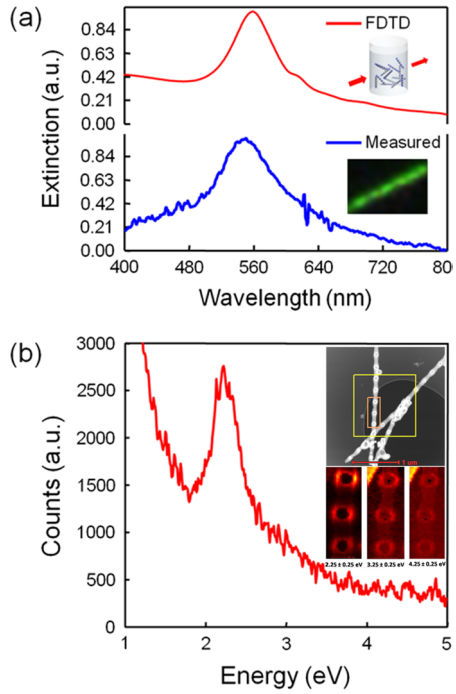

Figure 3. (a) Calculated (top) extinction spectrum of individual Au nanoparticle chains in isopropyl alcohol (IPA) solution and measured (bottom) extinction spectrum of the one-dimensional Au nanoparticle chain ensemble in IPA solution. Inset (top): Illustration of optical extinction measurement of a freestanding one-dimensional Au nanoparticle array chain ensemble in IPA solution. Inset (bottom): Dark-field microscopy images of the individual one-dimensional Au nanoparticle array; the green color agrees well with the plasmonic peak. (b) EELS of the individual one-dimensional Au nanoparticle array. The surface plasmon peak is at 2.25 eV. Inset (top): STEM image showing the area (orange box) in the vacuum region from which a spectrum image was obtained. The yellow box is the area that was used for drift correction during the experiment. Inset (bottom): Energy maps extracted from the spectrum image data with a window of width 0.5 eV centered at the indicated energy positions of 2.25 ± 0.25 eV (left), 3.25 ± 0.25 eV (middle), and 4.25 ± 0.25 eV (right). The energy intensity around the nanoparticle is enhanced at the resonance energy. Note: The halo only occurs along the axial direction because the thick 100 nm oxide in the radial direction prevents electrons from being collected.

onto a glass slide at a density low enough to isolate a single nanowire in the beam path. The array was illuminated with unpolarized white light from a tungsten–halogen lamp using an oil dark-field condenser (NA = 1.2–1.43). The light scattered from the arrays was then collected with a 100× objective lens and imaged with a digital CCD camera using an upright microscope (Nikon TE 200U). As shown in the inset of Figure 3a, the scattering image displays a uniform, strong green color at 520 to 570 nm, which is consistent with the position of the extinction peak, suggesting a dominant contribution of the scattering.

For comparison to theory, a finite difference time domain (FDTD) electromagnetic simulation was performed for a one-dimensional nanoparticle array composed of five spherical crystalline Au nanoparticles with a diameter of 80 nm and an interparticle spacing of 230 nm encapsulated in a SiO_2 nanowire with a diameter of 100 nm (n = 1.47) surrounded by IPA (n = 1.38). The incident electric field was swept from

DOI: 10.1021/acsnano.7b01479
ACS Nano 2017, 11, 5844–5852

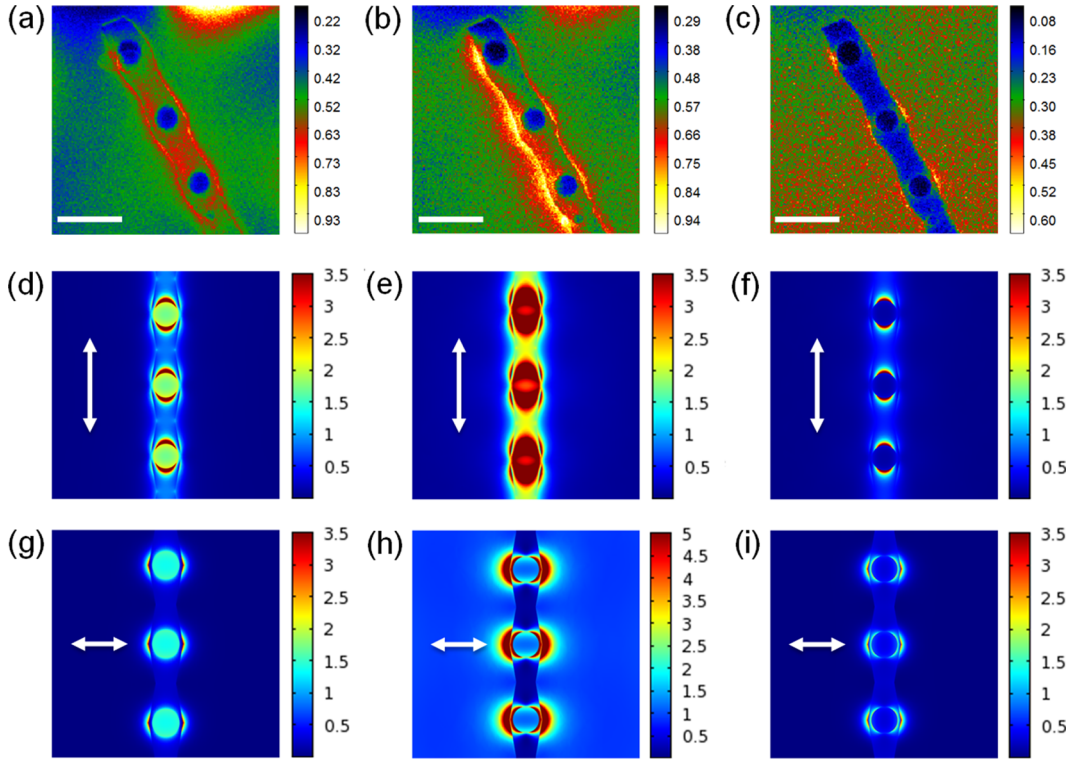

Figure 4. EFTEM images at (a) 1.6, (b) 2.2, and (c) 3.2 eV of an individual Au nanoparticle chain. Scale bar, 200 nm. Theoretical distribution of the electromagnetic field intensity $|E|^2$ at (d) 1.6, (e) 2.2, and (f) 3.2 eV of the chain with surface modulation when the light is incident along the chain;. Theoretical distribution of the electromagnetic field intensity $|E|^2$ at (g) 1.6, (h) 2.2, and (i) 3.2 eV of the chain with surface modulation when the light is incident perpendicular to the chain direction. The electric field is greatly enhanced around the plasmonic resonance energy from both the simulation and experiment result. Beyond or below the resonant energy, the electric field is not as strong as at the resonance energy. The arrow in the figures indicates the polarization direction.

parallel to vertical with respect to the long axis of the nanowire, and the average response is plotted in Figure 3a. The peak position in the simulated spectrum is 558 nm, which is red-shifted compared to the measurement. There are two possible reasons that can contribute to this slight difference in peak position: (1) the 12% variation in the nanoparticle diameter and interparticle spacing could contribute to the shift, and (2) the randomly oriented nanowires during the measurement can be viewed as disorder in the perfect one-dimensional array. As demonstrated previously,[39] disorder partially cancels the interparticle interaction, causing a blue-shift of the plasmon peak.

The plasmonic resonance at 558 nm corresponds to the coupled plasmonic dipolar modes of the Au nanoparticles. Because the nanoparticle diameters are larger than 50 nm, the nanoparticle can support a quadrupole resonance plasmonic mode.[40] To efficiently couple incident light into the quadrupolar mode, the phase of the incident light must change significantly across the nanoparticle.[41] The rapid spatial phase change occurs more easily at higher frequencies. Thus, the higher scattering intensity at short wavelengths is due to the excitation of the quadrupolar mode.[42] In addition, the transition between optical bands contributes to the strong extinction at shorter wavelengths. Applying a Lorentzian fit to the experimental and the simulated resonant responses gives a full-width at half-maximum (fwhm) of 76 and 60 nm for the experiment and simulation, respectively. The discrepancy in fwhm can be explained, in part, by the smaller number of nanoparticles included in the simulation as compared to experiment. Schatz *et al.*[40] showed theoretically that the peak width broadens as the number of nanoparticles increases. An array of five Au nanoparticles was used in the simulation, while the fabricated arrays contained 30 nanoparticles along each 6 μm long wire.

STEM[43] was used to characterize the plasmonic response of individual Au nanoparticles in the one-dimensional arrays. By scanning the electron beam probe with a spot size of only 1 nm, it is possible to excite and collect the EELS of individual nanoparticles. Figure 3b shows the EELS[44] along with the corresponding dark-field STEM image of the nanoparticle array that was collected from the same batch of nanowires used for extinction measurements. The EELS spectrum has a large peak at 2.25 eV (552 nm), which is consistent with the resonant peak positions in the extinction measurement and simulation. The energy map of the same nanoparticle array was collected to spatially resolve the energy distribution around each nanoparticle, as shown in the inset of Figure 3b. In the map collected at 2.25 eV with an energy window width of 0.5 eV, a uniform halo extends away from the surface of each nanoparticle in the array, which indicates there is an excitation of the surface plasmon at the resonant energy. The map extracted at 3.25 eV also shows weak intensity maxima adjacent to the nanoparticles corresponding to the gradual decay in the intensity around this energy region in the energy loss spectrum. We observe that the maxima in both maps are primarily located at localized regions surrounding the nanoparticles with no significant intensity in the region in between the nanoparticles.

Interparticle Plasmonic Excitation along Nanoparticle Arrays. To study the interparticle interaction along the array, the nanoparticles in the array were simultaneously excited by

DOI: 10.1021/acsnano.7b01479
ACS Nano 2017, 11, 5844−5852

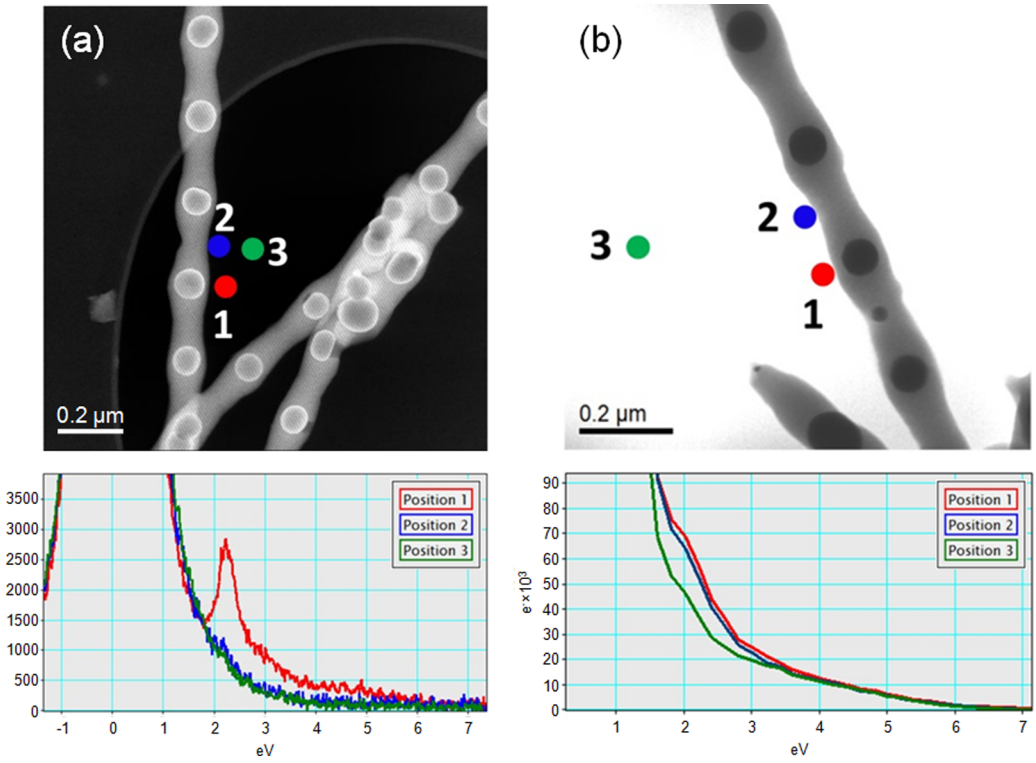

Figure 5. (a) STEM and (b) EFTEM images (top) with corresponding electron energy loss spectra (bottom), wherein the spectra have been extracted from positions 1, 2, and 3, identified by color in the respective images on top.

EFTEM with a parallel incident electron beam.[45] Figure 4a–c show raw EFTEM images collected for series of energy loss values centered at 1.6, 2.2, and 3.2 eV with a predefined energy width of 0.2 eV, further confirming that the resonance occurs at 2.2 eV (560 nm) and the plasmonic response of this structure is not sensitive to the surrounding environment (IPA *versus* vacuum). At the plasmonic resonance of 2.2 eV, a bright contrast is present both around and between the nanoparticles, indicating significant plasmonic enhancement in between the nanoparticles when multiple nanoparticles along the array are simultaneously excited. This is further supported by a comparison of the energy loss spectra from local positions in STEM-EELS and EFTEM spectrum images. Figure 5 shows STEM and TEM images along with the energy loss spectra from three different positions in a vacuum: the first being close to a nanoparticle (marked position 1 in red), the second, in between the nanoparticles (marked position 2 in blue), and third, away from these locations (marked position 3 in green). It is evident from the STEM-EELS results in Figure 5a that with the probe positioned in between the nanoparticles (*i.e.*, none of the nanoparticles in its vicinity are excited) the energy loss feature at 2.2 eV is significantly weaker than that obtained with the probe positioned close to the nanoparticles and that the overall spectrum is comparable to the background spectrum obtained with the probe positioned away from the nanoparticles. On the other hand, in the EFTEM mode in Figure 5b, where all nanoparticles are simultaneously excited, it is clear that the energy loss spectra extracted from positions near and in between the nanoparticles are almost identical and significantly higher than that extracted from a position away from the nanoparticles.

To interpret the EFTEM maps shown in Figure 4a–c and to correlate the optical plasmon mode[46] to the spatial distribution of the energy loss probability, electrodynamic simulations were performed on the individual one-dimensional nanoparticle arrays (COMSOL Multiphysics 4.2a, RF Module) of SiO_2-encapsulated, spherical crystalline Au nanoparticles with a diameter of 80 nm. The surface modulation was modeled as two SiO_2 cones with a height of 115 nm, a base diameter of 100 nm, and a top diameter of 60 nm mirrored at the center plane of the nanoparticle. The surrounding environment is a vacuum with $n = 1$. Figure 4d–i plot the distribution of the total electric field intensity $|E|^2$ at the center Au nanoparticles for incident energies of 1.6, 2.2, and 3.2 eV under the incident electric field parallel (Figure 4d–f) or perpendicular (Figure 4g–i) to the long-axis of the nanoparticle array. Strong agreement is observed between the simulated electromagnetic field distribution and the experimentally measured electron energy loss probability. The electron loss probability is related to the photonic local density of states (LDOS), and $|E|^2$ represents the scanning near-field optical microscopy intensity that is given by the LDOS.[47,48] At the resonant energy of 2.2 eV, the highest field intensity occurs around nanoparticles, and the field gradually decreases between adjacent nanoparticles. In contrast, the field intensities around and between the nanoparticles are weak when the incident energy is lower or higher than the resonance energy, indicating electromagnetic coupling between the nanoparticles near the resonant energy of an individual array. Furthermore, additional simulations shown in the Supporting Information (Figure S1) confirm the presence of a coupled resonant mode that is dependent on the interparticle spacing inside the nanowire. On the basis of these simulations, we observe that the results from the EFTEM maps in Figure 4a–c are consistent with the coupled resonant mode. However, an unambiguous experminental verification would require additional studies involving EELS-EFTEM studies on nano-

DOI: 10.1021/acsnano.7b01479
ACS Nano 2017, 11, 5844–5852

wires with interparticle spacing in the range corresponding to that indicated in Figure S1 in the Supporting Information.

FUTURE WORK AND OUTLOOK

To assess whether our method can be tuned to further decrease the ratio of the interparticle spacing to the particle diameter, thereby better inducing strong plasmonic couplings as well as understanding limitations of the process, endeavors to explore a wider range of process parameters are in progress. We also foresee that by removing the sonication process following the DRIE the vertically aligned nanowires can be maintained on the substrate, where further insight into the influence of the plasmonic Au nanoparticles on light−matter interactions would be revealed by polarized-light experiments. Furthermore, to better understand the morphological transitions from Au surface layers to Au nanowires to Au nanoparticle arrays, endeavors to evaluate fundamental parameters such as interfacial surface energies are also in progress.

CONCLUSIONS

In summary, a versatile nanofabrication approach was demonstrated to synthesize self-organized one-dimensional Au nanoparticle arrays encapsulated within freestanding SiO_2 nanowires by oxidation of Au-coated Si nanowires with surface modulation. This technique leads to a versatile platform for creating Au nanoparticle arrays with highly tailorable nanoparticle diameters and interparticle spacing. Specifically, the final nanoparticle diameter is determined by the volume of the Au coating, while the interparticle spacing is controlled by the modulation wavelength of the starting Si nanowire. The plasmonic responses of a randomly oriented population of arrays with nanoparticle diameters of 80 nm and interparticle spacings of 230 nm were collected using extinction measurements. A strong plasmonic peak was observed at 560 nm, which agrees well with the uniform green color in the far-field scattering images of individual one-dimensional nanoparticle arrays and the spectrum obtained by FDTD simulation. STEM-EELS further confirmed the plasmonic response and the uniform optical properties of the Au nanoparticles. EFTEM measurements showed plasmonic excitation along the one-dimensional nanoparticle array that is consistent with the existence of a coupled resonant mode predicted in simulations.

MATERIALS AND METHODS

Si Nanowire Synthesis and Au Film Coating. Free-standing Au nanoparticle arrays formed by oxidizing Au-coated Si nanowires with smooth surfaces can be used as a baseline for comparison to nanowires having surface modulation. The smooth-surface nanowires were grown by the VLS method using Au as a catalyst. The diameters of the starting nanowires in each batch varied from 20 to 50 nm, which contributes to a wide distribution in the final nanoparticle size. Prior to Au-enhanced oxidation, the catalyst metal was removed from the nanowire tips by selective wet chemical etching. The nanowires were removed from the substrate by sonication, dispersed onto a sacrificial Si_3N_4-coated Si substrate, and then coated with a uniform layer of 10 nm thick Au metal along the entire length of the nanowire. To ensure an intimate contact between the deposited Au layer and the Si nanowire, the nanowires were exposed to a brief buffer oxide etchant (JT Baker BOE 10:1) dip for 30 s to remove the native oxide before loading into the evaporator. After Au metal deposition, the nanowires were then thermally treated in a 15 in. diameter tube furnace at a temperature of 850 °C under O_2 with a flow rate of 0.8 L/min for 2 h.

Nanowire Surface Modulation. Surface-modulated Si nanowires were fabricated to study the effect of the starting nanowire diameter, modulation length, and Au layer thickness on the final nanoparticle diameter and interparticle spacing. Uniform diameter nanowires with three different modulation wavelengths of 230, 460, and 630 nm were fabricated using a modified DRIE process. The fabrication process began by forming a dense array of 6 μm long, vertically oriented Si nanowires with a nominal diameter of 1.2 μm diameter and a center-to-center pitch of 3 μm on a 3 in. diameter n^{++} Si substrate (resistivity <0.005 Ω·cm). The nanowire array features were patterned using projection lithography (GCA 8000 i-line stepper), and the pattern was transferred into the Si substrate using a modified DRIE (Alcatel Speeder 1000) process. During DRIE, the alternating etching and polymer deposition cycles were optimized to create the desired surface modulation (concave and convex segment regions) along the length of the nanowire.

Materials Characterization. The nanowire morphology studies were performed by FESEM and TEM imaging techniques using a Leo 1530 MERLIN operating at 5−20 kV and a TEM JEOL 2010F operating at 80 keV, respectively. The surface plasmon studies were performed by STEM, EELS, and EFTEM imaging techniques using the TEAM-0.5 (The National Center for Electron Microscopy, Berkeley, CA, USA) TEM, which was operated at an accelerating voltage of 80 kV. This system uses a high-brightness Schottky field emission electron source in combination with a Wein-filter monochromator and a high-resolution Gatan-Tridiem energy filter for EELS and EFTEM image acquisition. Under optimized experimental conditions, the energy spread in the electron beam was 0.12 eV (fwhm). The STEM-EELS experiments were performed using a convergent electron probe that was approximately 1 nm in diameter, and the energy-loss spectrum at each pixel was acquired with an energy dispersion of 0.01 eV/channel. The EFTEM images were acquired in the energy-loss spectral range 1−6 eV, using an energy selecting slit width of 0.2 eV. The images were acquired with a spatial sampling of 256 × 256 pixels and a field of view of 1 μm × 1 μm.

Optical Characterization. Numerical simulations for the cylindrical and spherical arrays were performed using a FDTD simulator (Lumerical). In the simulation setup, an array with five spherical Au particles was simulated. Each 80 nm diameter Au nanoparticle was encapsulated in SiO_2. The surface modulation was modeled as two 115 nm tall cones mirrored about the center plane of the nanoparticle, where the diameter at the base of the cone is 100 nm and the diameter at the top of the cone is 60 nm. The surrounding environment was IPA with a refractive index of 1.38. Perfectly matched layers were applied at the boundaries of the unit cell. The transmission spectra were collected using a power monitor that was placed 400 nm away from the bottom of the array plane. The absorption was calculated by subtracting the transmittance from unity. The electric field distribution of the nanoparticle array was simulated using a COMSOL Multiphysics 4.2 RF module. The simulation setup for the array geometry is the same as that used in the FDTD models. The surrounding environment was air with a refractive index of $n = 1$, and perfectly matched layers were applied at the boundaries of the unit cell. The $|E|^2$ was calculated and plotted.

ASSOCIATED CONTENT

Supporting Information

The Supporting Information is available free of charge on the ACS Publications website at DOI: 10.1021/acsnano.7b01479.

Etching conditions for the four types of surface-modulated Si nanowires used to create the one-dimensional Au nanoparticle arrays summarized in Table S1; Interplay between the interparticle coupling resonance and the resonant mode of each individual nanoparticle simulated in Figure S1 (PDF)

AUTHOR INFORMATION

Corresponding Authors

*E-mail (M. Kang): myungkoo@creol.ucf.edu.

DOI: 10.1021/acsnano.7b01479
ACS Nano 2017, 11, 5844−5852

*E-mail (T. S. Mayer): tsmayer@vt.edu.

ORCID

Myungkoo Kang: 0000-0003-4930-1683

Author Contributions

⊥M. Kang and Y. Yuwen contributed to this work equally.

Notes

The authors declare no competing financial interest.

ACKNOWLEDGMENTS

The authors acknowledge funding from NSF MRSEC No. DMR-0213623 and ARO No. W911 NF-09-1-0140. The STEM-EELS and EFTEM experiments were performed at the National Center for Electron Microscopy, which is partially supported by the Director, Office of Science, Office of Basic Energy Science, of the U.S. Department of Energy under Contract No. DE-AC03-76SF00098. The authors thank Dr. P. Nimmatoori, Dr. B. Liu, N. Dellas, Dr. J. Redwing, Dr. S. Mohney, Dr. C. M. Schwarz, and L. Sisken for the growth and characterization of VLS Si nanowires and useful discussions.

REFERENCES

(1) Intartaglia, R.; Beke, S.; Moretti, M.; De Angelis, F.; Diaspro, A. Fast and Cost-Effective Fabrication of Large-Area Plasmonic Transparent Biosensor Array. *Lab Chip* **2015**, *15*, 1343.

(2) Zhang, K.; Zhao, J.; Ji, J.; Li, Y.; Liu, B. Quantitative Label-Free and Real-Time Surface-Enhanced Raman Scattering Monitoring of Reaction Kinetics Using Self-Assembled Bifunctional Nanoparticle Arrays. *Anal. Chem.* **2015**, *87*, 8702.

(3) Maier, S. A.; Kik, P. G.; Atwater, H. A. Observation of Coupled Plasmon-Polariton Modes in Au Nanoparticle Chain Waveguides of Different Lengths: Estimation of Waveguide Loss. *Appl. Phys. Lett.* **2002**, *81*, 1714.

(4) Edel, J. B.; Kornyshev, A. A.; Urbakh, M. Self-Assembly of Nanoparticle Arrays for Use as Mirrors, Sensors, and Antennas. *ACS Nano* **2013**, *7*, 9526.

(5) Li, Z.; Butun, S.; Aydin, K. Touching Gold Nanoparticle Chain Based Plasmonic Antenna Arrays and Optical Metamaterials. *ACS Photonics* **2014**, *1*, 228.

(6) Zou, S. L.; Janel, N.; Schatz, G. C. Silver Nanoparticle Array Structures that Produce Remarkably Narrow Plasmon Lineshapes. *J. Chem. Phys.* **2004**, *120*, 10871.

(7) Wang, D.; Ji, R.; Schaaf, P. Formation of Precise 2D Au Particle Arrays *via* Thermally Induced Dewetting on Pre-Patterned Substrates. *Beilstein J. Nanotechnol.* **2011**, *2*, 318.

(8) Lin, C. H.; Jiang, L.; Chai, Y. H.; Xiao, H.; Chen, S. J.; Tsai, H. L. A Method to Fabricate 2D Nanoparticle Arrays. *Appl. Phys. A: Mater. Sci. Process.* **2010**, *98*, 855.

(9) Giermann, A. L.; Thompson, C. V. Solid-State Dewetting for Ordered Arrays of Crystallographically Oriented Metal Particles. *Appl. Phys. Lett.* **2005**, *86*, 121903.

(10) Lian, J.; Wang, L.; Sun, X.; Yu, Q.; Ewing, R. C. Patterning Metallic Nanostructures by Ion-Beam-Induced Dewetting and Rayleigh Instability. *Nano Lett.* **2006**, *6*, 1047.

(11) Rack, P. D.; Guan, Y.; Fowlkes, J. D.; Melechko, A. V.; Simpson, M. L. Pulsed Laser Dewetting of Patterned Thin Metal Films: A Means of Directed Assembly. *Appl. Phys. Lett.* **2008**, *92*, 223108.

(12) Oh, Y.; Ross, C. A.; Jung, Y. S.; Wang, Y.; Thompson, C. V. Cobalt Nanoparticle Arrays Made by Templated Solid-State Dewetting. *Small* **2009**, *5*, 860.

(13) Wu, Y.; Fowlkes, J. D.; Rack, P. D.; Diez, J. A.; Kondic, L. On the Breakup of Patterned Nanoscale Copper Rings into Droplets *via* Pulsed-Laser-Induced Dewetting: Competing Liquid-Phase Instability and Transport Mechanisms. *Langmuir* **2010**, *26*, 11972.

(14) Ye, J.; Thompson, C. V. Templated Solid-State Dewetting to Controllably Produce Complex Patterns. *Adv. Mater.* **2011**, *23*, 1567.

(15) Ruffinoa, F.; Grimaldi, M. G. Template-Confined Dewetting of Au and Ag Nanoscale Films on Mica Substrate. *Appl. Surf. Sci.* **2013**, *270*, 697.

(16) Kumar, A.; Mandal, S.; Mathew, S. P.; Selvakannan, P. R.; Mandale, A. B.; Chaudhari, R. V.; Sastry, M. Benzene-and Anthracene-Mediated Assembly of Gold Nanoparticles at the Liquid−Liquid Interface. *Langmuir* **2002**, *18*, 6478.

(17) Kuznetsov, A. I.; Evlyukhin, A. B.; Goncalves, M. R.; Reinhardt, C.; Koroleva, A.; Arnedillo, M. L.; Kiyan, R.; Marti, O.; Chichkov, B. N. Laser Fabrication of Large-Scale Nanoparticle Arrays for Sensing Applications. *ACS Nano* **2011**, *5*, 4843.

(18) Gumennik, A.; Wei, L.; Lestoquoy, G.; Stolyarov, A. M.; Jia, X.; Rekemeyer, P. H.; Smith, M. J.; Liang, X.; Grena, B. J. -B.; Johnson, S. G.; Gradecak, S.; Abouraddy, A. F.; Joannopoulos, J. D.; Fink, Y. Silicon-in-Silica Spheres *via* Axial Thermal Gradient in-Fibre Capillary Instabilities. *Nat. Commun.* **2013**, *4*, 2216.

(19) Slaughter, L. S.; Wang, L.; Willingham, B. A.; Olson, J. M.; Swanglap, P.; Dominguez-Medinaab, S.; Link, S. Plasmonic Polymers Unraveled through Single Particle Spectroscopy. *Nanoscale* **2014**, *6*, 11451.

(20) Yang, M.; Chen, G.; Zhao, Y.; Silber, G.; Wang, Y.; Xing, S.; Han, Y.; Chen, H. Mechanistic Investigation into the Spontaneous Linear Assembly of Gold Nanospheres. *Phys. Chem. Chem. Phys.* **2010**, *12*, 11850.

(21) Kolb, F. M.; Berger, A.; Hofmeister, H.; Pippel, E.; Gosele, U.; Zacharias, M. Periodic Chains of Gold Nanoparticles and the Role of Oxygen during the Growth of Silicon Nanowires. *Appl. Phys. Lett.* **2006**, *89*, 173111.

(22) Karim, S.; Toimil-Molares, M. E.; Balogh, A. G.; Ensinger, W.; Cornelius, T. W.; Khan, E. U.; Neumann, R. Morphological Evolution of Au Nanowires Controlled by Rayleigh Instability. *Nanotechnology* **2006**, *17*, 5954.

(23) Wu, J. S.; Dhara, S.; Wu, C. T.; Chen, K. H.; Chen, Y. F.; Chen, L. C. Growth and Optical Properties of Self-Organized Au_2Si Nanospheres Pea-Podded in a Silicon Oxide Nanowire. *Adv. Mater.* **2002**, *14*, 1847.

(24) Hu, M.; Chen, H.; Shen, C.; Hong, L.; Huang, B.; Chen, K.; Chen, L. Photosensitive Gold-Nanoparticle-Embedded Dielectric Nanowires. *Nat. Mater.* **2006**, *5*, 102.

(25) Fletcher, N. H.; Elliman, R. G.; Kim, T. Gold Bead-Strings in Silica Nanowires: A Simple Diffusion Model. *Nanotechnology* **2009**, *20*, 085613.

(26) Gentile, A.; Ruffino, F.; Boninelli, S.; Grimaldi, M. G. Silica Nanowire-Au Nanoparticle Pea-Podded Composites: Synthesis and Structural Analyses. *Thin Solid Films* **2015**, *589*, 755.

(27) Hu, W.; Liu, B.; Dellas, N. S.; Eichfeld, S. M.; Mohney, S. E.; Redwing, J. M.; Mayer, T. S. Lithography-Free Synthesis of Freestanding Gold Nanoparticle Arrays Encapsulated within Dielectric Nanowires. *Proc. SPIE* **2010**, *7610*, 76100V−1.

(28) Kendrick, C. E.; Yoon, H. P.; Yuwen, Y. A.; Barber, G. D.; Shen, H.; Mallouk, T. E.; Dickey, E. C.; Mayer, T. S.; Redwing, J. M. Radial Junction Silicon Wire Array Solar Cells Fabricated by Gold-Catalyzed Vapor-Liquid-Solid Growth. *Appl. Phys. Lett.* **2010**, *97*, 143108.

(29) Hiraki, A.; Nicolet, M. A.; Mayer, J. W. Low-Temperature Migration of Silicon in Thin Layers of Gold and Platinum. *Appl. Phys. Lett.* **1971**, *18*, 178.

(30) Qin, Y.; Liu, L.; Yang, R.; Gosele, U.; Knez, M. General Assembly Method for Linear Metal Nanoparticle Chains Embedded in Nanotubes. *Nano Lett.* **2008**, *8*, 3221.

(31) Wu, Y.; Hsieh, C.; Chen, P.; Li, J.; Chou, L.; Chen, L. Plasmon Resonance Spectroscopy of Gold-in-Gallium Oxide Peapod and Core/Shell Nanowires. *ACS Nano* **2010**, *3*, 1393.

(32) Xu, J.; Zhu, Y.; Zhu, J.; Jiang, W. Ultralong Gold Nanoparticle/Block Copolymer Hybrid Cylindrical Micelles: A Strategy Combining Surface Templated Self-Assembly and Rayleigh Instability. *Nanoscale* **2013**, *5*, 6344.

(33) Ruffino, F.; Pugliara, A.; Carria, E.; Bongiorno, C.; Spinella, C.; Grimaldi, M. G. Formation of Nanoparticles from Laser Irradiated Au

DOI: 10.1021/acsnano.7b01479
ACS Nano 2017, 11, 5844−5852

Thin Film on SiO_2/Si: Elucidating the Rayleigh-Instability Role. *Mater. Lett.* **2012**, *84*, 27.
(34) Nichols, F. A.; Mullins, W. W. Morphological Changes of a Surface of Revolution due to Capillarity-Induced Surface Diffusion. *J. Appl. Phys.* **1965**, *36*, 1826.
(35) Power, J. D.; Glaeser, A. M. Orientation Effects on the High-Temperature Morphological Evolution of Pore Channels in Sapphire. *J. Am. Ceram. Soc.* **2000**, *83*, 2297.
(36) Fu, Y. Q.; Colli, A.; Fasoli, A.; Luo, J. K.; Flewitt, A. J.; Ferrari, A. C.; Milne, W. I. Deep Reactive Ion Etching as a Tool for Nanostructure Fabrication. *J. Vac. Sci. Technol. B* **2009**, *27*, 1520.
(37) Hu, W. Nanowire-Based Devices for Electronic and Optical Applications: Solution-Gated Silicon Nanowire Field Effect Transistors and One-Dimensional Gold Nanoparticle Arrays. Ph.D. Thesis, Pennsylvania State University, 2010.
(38) Kreibig, U.; Vollmer, M. *Optical Properties of Metal Clusters*; Springer-Verlag: Berlin, 1995.
(39) Auguié, B.; Barnes, W. L. Diffractive Coupling in Gold Nanoparticle Arrays and the Effect of Disorder. *Opt. Lett.* **2009**, *34*, 401.
(40) Zou, S. L.; Schatz, G. C. Theoretical Studies of Plasmon Resonances in One-Dimensional Nanoparticle Chains: Narrow Lineshapes with Tunable Widths. *Nanotechnology* **2006**, *17*, 2813.
(41) Burrows, C. P.; Barnes, W. L. Large Spectral Extinction due to Overlap of Dipolar and Quadrupolar Plasmonic Modes of Metallic Nanoparticles in Arrays. *Opt. Express* **2010**, *18*, 3187.
(42) Rodríguez-Fernández, J.; Pérez-Juste, J.; García de Abajo, F. J.; Liz-Marzán, L. M. Seeded Growth of Submicron Au Colloids with Quadrupole Plasmon Resonance Modes. *Langmuir* **2006**, *22*, 7007.
(43) Raza, S.; Kadkhodazadeh, S.; Christensen, T.; Di Vece, M.; Wubs, M.; Mortensen, N. A.; Stenger, N. Multipole Plasmons and their Disappearance in Few-Nanometre Silver Nanoparticles. *Nat. Commun.* **2015**, *6*, 8788.
(44) Wu, Y.; Li, G.; Cherqui, C.; Bigelow, N. W.; Thakkar, N.; Masiello, D. J.; Camden, J. P.; Rack, P. D. Electron Energy Loss Spectroscopy Study of the Full Plasmonic Spectrum of Self-Assembled Au−Ag Alloy Nanoparticles: Unraveling Size, Composition, and Substrate Effects. *ACS Photonics* **2016**, *3*, 130.
(45) Schaffer, B.; Hohenester, U.; Trugler, A.; Hofer, F. High Resolution Surface Plasmon Imaging of Gold Nanoparticles by Energy-Filtered Transmission Electron Microscopy. *Phys. Rev. B: Condens. Matter Mater. Phys.* **2009**, *79*, 041401.
(46) Guiton, B. S.; Iberi, V.; Li, S.; Leonard, D. N.; Parish, C. M.; Kotula, P. G.; Varela, M.; Schatz, G. C.; Pennycook, S. J.; Camden, J. P. Correlated Optical Measurements and Plasmon Mapping of Silver Nanorods. *Nano Lett.* **2011**, *11*, 3482.
(47) Garcia De Abajo, F. J. Optical Excitations in Electron Microscopy. *Rev. Mod. Phys.* **2010**, *82*, 209.
(48) Caselli, N.; La China, F.; Bao, W.; Riboli, F.; Gerardino, A.; Li, L.; Linfield, E. H.; Pagliano, F.; Fiore, A.; Schuck, P. J.; Cabrini, S.; Weber-Bargioni, A.; Gurioli, M.; Intonti, F. Deep-Subwavelength Imaging of both Electric and Magnetic Localized Optical Fields by Plasmonic Campanile Nanoantenna. *Sci. Rep.* **2015**, *5*, 9606.

DOI: 10.1021/acsnano.7b01479
ACS Nano 2017, 11, 5844−5852